International Journal of Applied Electromagnetics and Mechanics 13 (2001/2002) 229–234
IOS Press

Efficiency analysis of induction motor considering rotor and stator surface loss caused by rotor movement

Katsumi Yamazaki
Department of Electrical Engineering, Chiba Institute of Technology, 2-17-1 Tsudanuma, Narashino, Chiba 275-0016, Japan
Tel.: +81 47 478 0373; Fax: +81 47 478 0379; E-mail: yamazaki@pf.it-chiba.ac.jp

Abstract. This paper presents a method to calculate efficiency of induction motorsconsidering stray losses caused by stator and rotor slot ripple. The harmonic electromagnetic fields are calculated by the combined 3D-2D nonlinear time-stepping finite element analysis considering movement of the rotor to estimate the harmonic copper and iron losses. The calculated losses and efficiency is compared with the experimental results. It is clarified that the losses concentrate at the surface of the stator and the rotor core and that the consideration of the time-harmonics caused by the rotor movement is indispensable to estimate the losses and the efficiency of the motor.

1. Introduction

Induction motors are widely applied to the industries as general-purpose motors. They consume a large percent of electrical demands in many countries. Owing to the environmental problems, estimations of the motor losses and improvement of the efficiency become important subjects. It is well known that the time variations of magnetic fields near the air gap of induction motors often include much time-harmonics caused by the slot ripple. They often produce the stray losses (the additional load losses), which are difficult to estimate before manufacturing [1]. In this paper, we investigate the loss distribution and calculate the efficiency of the motor using the combined 3D-2D nonlinear time-stepping finite element analysis considering movement of the rotor [2]. It is clarified that the losses concentrate at the surface of the stator and the rotor core and that the consideration of the rotor movement is indispensable to estimate the efficiency of the motor.

2. Calculation method

Figure 1 shows the procedure to calculate the losses and the efficiency of the induction motor. The calculation method consists of two steps.

First, the electromagnetic field of the motor is analyzed by the nonlinear time-stepping finite element analysis with the primary voltage equation. As we will discuss in Chapter 3, much time-steps are required to estimate the losses of the motor. Thus, we apply combined 3D-2D formulation [2] to reduce

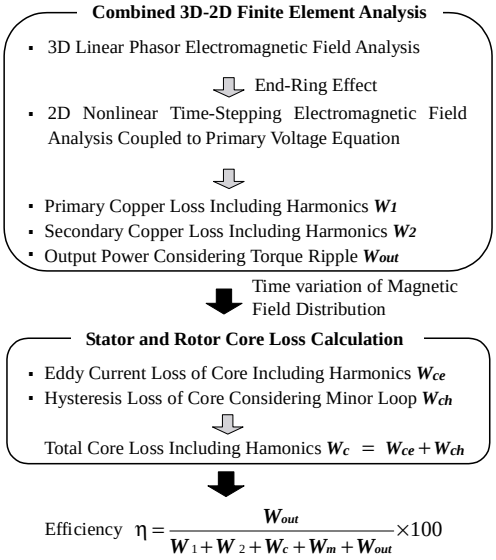

Fig. 1. Procedure to calculate losses and efficiency.

the calculation time. In the formulation, the end-ring effects of the motor are estimated by the linear phasor (frequency domain) analysis whose governing equations are

$$\nabla \times \left(\frac{1}{\mu}\nabla \times \boldsymbol{A}_{3D}\right) = \boldsymbol{J} + \sigma(-js\omega \boldsymbol{A}_{3D} - \nabla\phi) \tag{1}$$

$$\nabla \times \{\sigma(-js\omega \boldsymbol{A}_{3D} - \nabla\phi)\} = 0 \tag{2}$$

where $\boldsymbol{A}_{3D}, \phi$ are the magnetic vector and electric scalar potential used in the 3D analysis, $s\omega$ is the slip angular frequency, μ is the permeability, σ is the conductivity of the secondary conductor.

The characteristics of the induction motor is calculated by the 2D nonlinear time-stepping analysis with the bar conductivity σ' modified by the 3D analysis, that is

$$-\nabla\left(\frac{1}{\mu}\nabla A_z\right) = J - \sigma'\frac{\partial A_z}{\partial t} \tag{3}$$

where

$$\sigma' = (1-k)\sigma \tag{4}$$

k is the ratio of the voltage drop of the end-rings to the total secondary induced voltage calculated by the 3D analysis. The primary voltage equations considering star connection of the motor are coupled to Eq. (3) because the known quantities of the analysis are UV and VW line voltages [3].

The finite element meshes of the rotor and the stator are connected automatically due to the rotor angle in order to consider the time-harmonics caused by the movement of the rotor slots. As a result, we can obtain the primary copper loss (stator coil joule loss) W_1 and secondary copper loss (rotor cage eddy current loss) W_2 with the consideration of the time-harmonics as follows

$$W_1 = \frac{1}{T}\int_0^T \left(RI_{1U}^2 + RI_{1V}^2 + RI_{1W}^2\right) dt \tag{5}$$

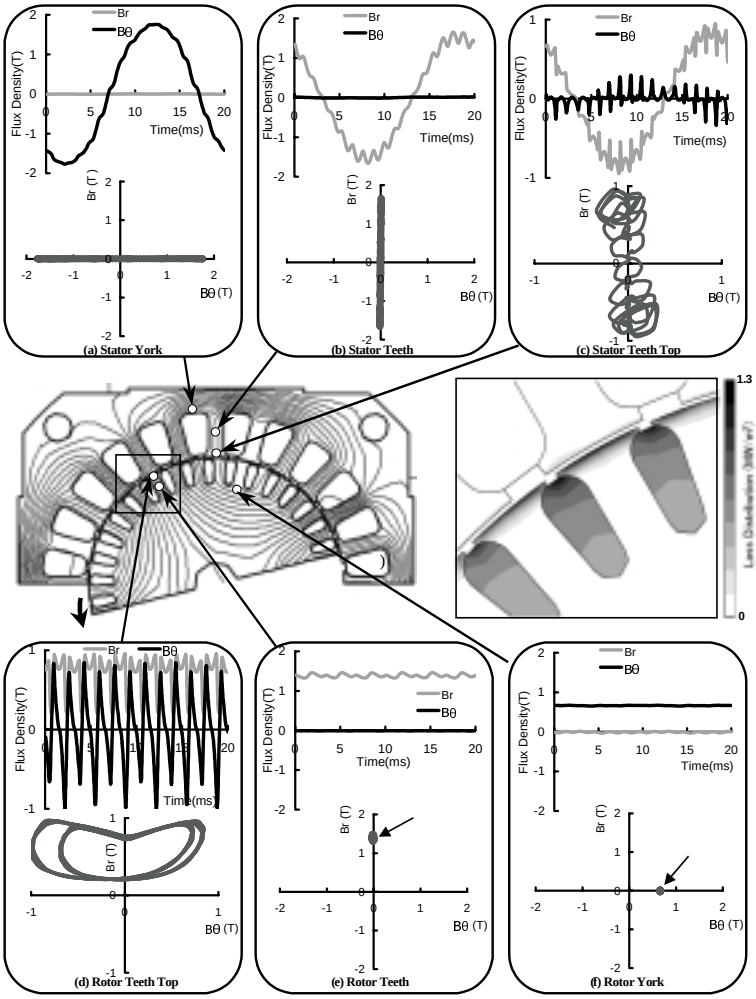

Fig. 2. Space distribution and time variation of magnetic field and loss distribution (no load condition, slip $= 0$).

$$W_2 = \frac{1}{T}\int_0^T \int \frac{|\boldsymbol{J}_2|^2}{\sigma} dvdt \tag{6}$$

where T is the time interval and R is the primary coil resistance, I_1 is the primary coil current, $\boldsymbol{J}_2$ is the secondary current density. At this first step of the procedure, the effects of the eddy currents and hysteresis phenomena of the stator and rotor cores are neglected.

Second, the core losses of the stator and rotor are calculated from the time variation of the magnetic fields obtained by the first step. Following assumptions are introduced to calculate the harmonic iron losses.

(a) The total iron loss is assumed as the sum of the losses that are caused by the radial component B_r and peripheral component B_θ, respectively. (Two-dimensional magnetic properties of the core [4] are neglected.)
(b) The major and the minor histeresys loops are assumed as similar in shape.
(c) The total hysteresis loss is assumed as the sum of the area of all hysteresis loops [5–7].

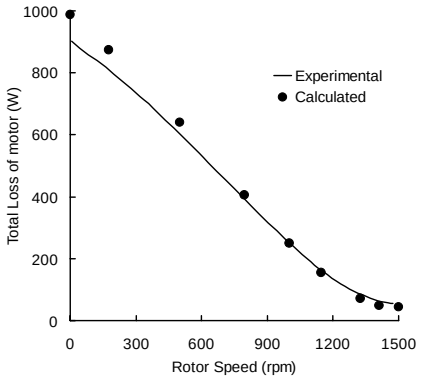

Fig. 3. Experimental and calculated total losses of motor.

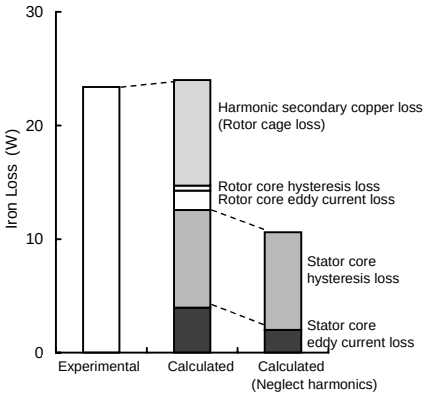

Fig. 4. Experimental and calculated iron losses (slip $= 0$).

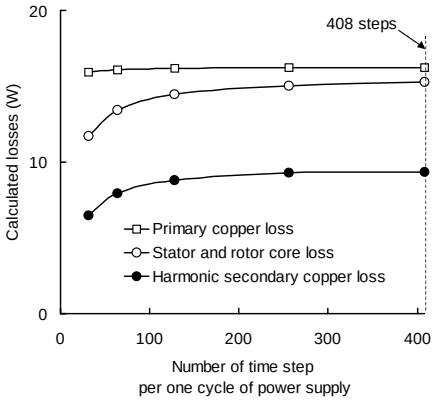

Fig. 5. Variation of calculated losses due to time-step.

Due to these assumptions, we can calculate the eddy current and hysteresis losses of the core W_{ce} and W_{ch} as

$$W_{ce} = \frac{K_e D}{2\pi^2} \int_{\text{iron}} \frac{1}{N} \sum_{k=1}^{N} \left\{ \left(\frac{B_r^{k+1} - B_r^k}{\Delta t} \right)^2 + \left(\frac{B_\theta^{k+1} - B_\theta^k}{\Delta t} \right)^2 \right\} dv \tag{7}$$

$$W_{ch} = \frac{K_h D}{T} \sum_{i=1}^{NE} \frac{\Delta V_i}{2} \left(\sum_{j=1}^{{N_{pr}}^i} (B_{mr}^{ij})^2 + \sum_{j=1}^{{N_{P\theta}}^i} (B_{m\theta}^{ij})^2 \right) \tag{8}$$

where D is the density of the core, K_e, K_h are the experimental constant by Epstein frame, N is the number of time step per one time period, Δt is the time interval, ΔV_i is the volume of i-th finite element, $B_{mr}^{ij}, B_{m\theta}^{ij}$ are the amplitude of each hysteresis loop.

3. Results

The proposed procedure is applied to the IEEJ induction motor K model [3], which is the 200 W class aluminum cage induction motor driven by a sinusoidal 100 V power supply. The number of the

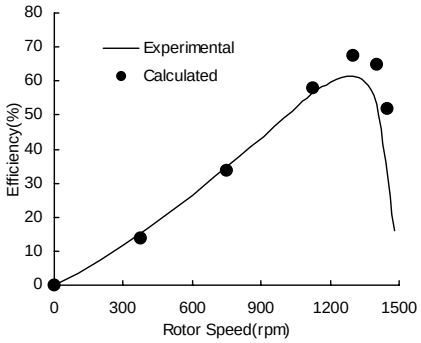

Fig. 6. Experimental and calculated efficiency of motor.

finite elements is 74,400 tetrahedron edge-elements for the 3D linear phasor analysis and 19,678 triangle elements in the 2D nonlinear time-stepping analysis, respectively. The number of time step is 256 per one cycle of power supply.

Figure 2 shows results of the flux distribution, time-variation of the flux density and the loss distribution at no load condition (1500 rpm, slip $= 0$). The magnetic fields at the stator yoke and stator teeth (a), (b) are nearly alternating fields of peripheral and radial direction, respectively. The waveforms of B_r and B_θ involve much time-harmonics near the air gap due to the movement of rotor slots. As a result, the locus of B_r and B_θ at top of the stator slot tooth (c) shows complex variation. The field at the top of the rotor slot tooth (d) also involves much time-harmonics due to the stator slot ripple. In this case, the locus of B_r and B_θ shows high frequency rotational magnetic field. As a result, the core loss concentrates at the rotor surface in this case. On the other hand, the magnetic fields at the rotor tooth and yoke (e), (f) are nearly DC fields of radial and peripheral direction, respectively because of slip $= 0$. The loss of the bar, that is, the secondary copper loss also concentrates at the surface due to the skin effect of the harmonic secondary currents.

Figure 3 shows the experimental and calculated total losses of the motor due to the rotor speed. The results agree well. It can be considered that the accuracy of the analysis is enough.

Figure 4 shows the experimental and calculated iron losses at no load condition. In the experiment, the iron loss W_i is determined due to the classical electric machine theory as follows

$$W_i = W_{\mathrm{noload}} - W_1 - W_m \tag{9}$$

where W_{noload} is the measured no load loss that is shown in the experimental result of Fig. 3 at 1500 rpm, W_1 is the measured primary copper loss and the W_m is the mechanical loss. In this classical definition, W_i includes not only core loss W_c but also harmonic copper loss W_2. Figure 4 indicate that the experimental iron loss W_i agrees well with the sum of the calculated harmonic secondary copper loss and the core losses $W_i + W_2$.

Figure 4 also shows the calculated result without the consideration of the harmonics caused by the rotor movement. When we neglect the harmonics, the secondary copper loss and the rotor core losses are assumed as zero at slip $= 0$. In addition, the calculated stator core losses are underestimated due to the neglect of the harmonics of the magnetic field. As a result, only less than half of the iron loss is estimated in this case. It is clarified that the consideration of the rotor movement is indispensable to estimate the losses of the motor and that the harmonic secondary copper loss and the rotor core losses at slip $= 0$ are not negligible.

Figure 5 shows the variation of the calculated core loss, primary and secondary copper losses at no load condition due to the number of time-steps of the time-stepping analysis. Figure 5 indicates that much time-steps are required for the accurate estimation of the core loss and the secondary copper loss (rotor cage eddy current loss) because much time-harmonics is included in the electromagnetic fields in the motor. On the other hand, the calculated primary copper loss, which is obtained from the primary coil currents, is not so much influenced by the number of the time-steps because the harmonics included in the primary coil currents are relatively small.

The results of 408 steps at one cycle of power supply in Figure 5 are obtained without the change of the finite element mesh at each time-step because the number of elements at one-pole pair along by the air-gap is 408. On the other hand, other results are obtained with the mesh changes. Figure 5 indicates that the effects of the mesh distortion can be considered as negligible because the results at 408 and 256 steps are almost identical. The calculation time is about 5 hours using PENTIUM 933 MHz PC at one cycle of power supply with 256 steps.

Figure 6 shows the calculated and experimental efficiency. The results agree well. The reasons of the slight overestimation of the calculated result can be considered as follows.

(a) Neglect of the effects of the eddy currents and hysteresis phenomena of the stator and rotor cores in the finite element analysis, which is the first step of the calculation procedure shown in Fig. 1.
(b) Neglect of the two-dimensional magnetic properties.

4. Conclusions

The losses and the efficiency of the induction motor are analyzed with the consideration of stray losses caused by the stator and rotor slot ripple. It is clarified that the losses concentrate at the surface of the stator and the rotor core and that the consideration of the time-harmonics caused by the rotor movement is indispensable to estimate the losses and the efficiency of the motor. The combined 3D-2D finite element formulation is useful from the point of the calculation time because much time steps are required for the correct estimation of the harmonic secondary copper loss and the core loss. Further work is required to consider the core loss and the 2D magnetic properties directly by the electromagnetic analysis with the estimation of the time-harmonics, which requires vast calculation time.

References

[1] B. Slates, P. Van Roy and R. Belmans, Energy Efficiency of Induction Machines, *Proc. ICEM2000* **3** (2000), 1503.
[2] K. Yamazaki, Induction Motor Analysis Considering both Harmonics and End Effects Using Combination of 2D and 3D Finite Element Method, *IEEE Trans. Energy Conversion* **14**(3) (1999), 698.
[3] K. Yamazaki and S. Shinfuku, Combined 3D-2D Finite Element Analysis Considering Variation of Neutral Point Potential in Star Connection, *IEEE Trans. Magn* (in press).
[4] M. Enokizono, T. Todaka and K. Okamoto, A Numerical Simulation of Induction Motor By Using Two-Dimensional Magnetic Properties, *Proc. CEFC2000* (2000), 182.
[5] J.D. Lavers, P.P. Bringer and H. Hollitscher, A simple method of estimating the minor loop hysteresis loss in thin lamination, *IEEE Trans. Magn.* **14**(5) (1978), 386.
[6] S.L. Ho, W.N. Fu and H.C. Wong, Estimation of Stray Losses of Skewed Rotor Induction Motors Using Coupled 2-D and 3-D Time Stepping Finite Element Methods, *IEEE Trans. Magn* **34**(5) (1998), 3102.
[7] N. Sadowski, J.P.A. Bastos, M.V. Ferreira Da Luz, P. Kuo-Peng and M. Lajoie-Mazenc, The Rain-Flow Method for Evaluation of Iron Losses in Electrical Machines, *IEEE Trans. Magn.* **36**(4) (2000), 1926.